Channel Estimation for Practical IRS-Assisted OFDM Systems

Wanning Yang†, Hongyu Li†, Ming Li†, Yang Liu†, and Qian Liu‡
†School of Information and Communication Engineering
Dalian University of Technology, Dalian, Liaoning 116024, China
E-mail: {yangwanning, hongyuli}@mail.dlut.edu.cn, {mli, yangliu613}@dlut.edu.cn
‡School of Computer Science and Technology
Dalian University of Technology, Dalian, Liaoning 116024, China
E-mail: qianliu@dlut.edu.cn

***Abstract*—Intelligent reflecting surface (IRS), composed of a large number of hardware-efficient passive elements, is deemed as a potential technique for future wireless communications since it can adaptively enhance the propagation environment. In order to effectively utilize IRS to achieve promising beamforming gains, the problem of channel state information (CSI) acquisition needs to be carefully considered. However, most recent works assume to employ an ideal IRS, i.e., each reflecting element has constant amplitude, variable phase shifts, as well as the same response for the signals with different frequencies, which will cause severe estimation error due to the mismatch between the ideal IRS and the practical one. In this paper, we study channel estimation in practical IRS-aided orthogonal frequency division multiplexing (OFDM) systems with discrete phase shifts. Different from the prior works which assume that IRS has an ideal reflection model, we perform channel estimation by considering amplitude-phase shift-frequency relationship for the response of practical IRS. Aiming at minimizing normalized-mean-square-error (NMSE) of the estimated channel, a novel IRS time-varying reflection pattern is designed by leveraging the alternating optimization (AO) algorithm for the case of using low-resolution phase shifters. Moreover, for the high-resolution IRS cases, we provide another practical reflection pattern scheme to further reduce the complexity. Simulation results demonstrate the necessity of considering practical IRS model for channel estimation and the effectiveness of our proposed channel estimation methods.**

***Index Terms*—Intelligent reflecting surface (IRS), orthogonal frequency division multiplexing (OFDM), channel estimation, normalized-mean-square-error (NMSE), reflection pattern design.**

I. Introduction

Intelligent reflecting surface (IRS), as a promising technology to enhance propagation in wireless communication systems, has recently attracted drastic attention. The IRS is generally composed of a great number of energy-efficient passive elements [1], e.g., phase shifters, which can dynamically modify the phase or/and amplitude of the incident signal and effectively improve channel/beamforming gain without additional hardware cost. Furthermore, IRS can be easily mounted on or removed from environment objects for deployment/replacement owing to its conformal geometry and light weight property [2]. Appealed by the advantage of IRS, the application of IRS for a wide range of communication scenarios, e.g. data transmission rate improvement [3], coverage enhancement [2], and secure communication [4], has been intensively investigated.

To completely achieve the appealing advantages brought by the IRS, the issue of accurate channel state information (CSI) acquisition needs to be deliberately considered. However, channel estimation in IRS-assisted systems is a challenging task because it is very difficult for passive elements to sense the channels. Now the mainstream channel estimation for IRS-assisted systems is twofold: *i)* Active estimation, i.e., equipping the IRS with some active sensors; *ii)* passive estimation, i.e., pre-defining the reflection pattern to estimate the CSI. Generally, the latter one (i.e., the passive estimation) is of much more superiority because it is more cost-effective and easier to implement. Recently, there exist many works for passive estimation in IRS-aided systems with narrowband channels [5]-[10]. However, for wideband wireless communication systems, the problem will become quite complicated due to more channel coefficients to be estimated, which are brought by the multi-path delay spread. Up to now, only limited work focuses on AP-IRS-user cascade channel estimation in IRS-aided orthogonal frequency division multiplexing (OFDM) systems. Specifically in [11], an ON/OFF-based protocol (i.e., only small portion of IRS elements are on at each time slot) was firstly proposed, however, which will incur a large normalized-mean-square-error (NMSE) because the array gain cannot be fully exploited. In [12], the authors proposed a discrete Fourier transforms (DFT)-based reflecting pattern design scheme to reduce the estimation errors greatly as compared to the ON/OFF-based protocol. Moreover, the authors in [13] proposed a fast channel estimation scheme with reduced OFDM symbol duration to further reduce training overhead. Recently, machine learning (ML) based channel estimation strategies have also been investigated in [14] to improve the channel estimation performance.

However, all the above works assume IRS has an ideal reflection model, i.e., constant amplitude, variable phase shifts, as well as the same response for the signals with different frequencies, which is impractical due to the real world hardware limitation. Thus, it is very necessary to adopt a novel method to execute channel estimation based on the practical IRS model

and further reduce NMSE of the estimated channels in IRS-assisted OFDM systems.

In this paper, we consider a simple point-to-point IRS-assisted OFDM system and perform channel estimation based on our proposed practical IRS model. Next, aiming at minimizing the NMSE, we properly design an IRS time-varying reflection pattern for the case of using low-resolution phase shifters by leveraging alternating optimization (AO) technique. Then, for high-resolution IRS cases, we propose a practical reflection pattern design scheme with lower computational complexity. Finally, simulation results verify the necessity of taking the practical IRS model into consideration and the priority of our proposed channel estimation methods.

Notations: $(\cdot)^T$, $(\cdot)^H$, and $(\cdot)^{-1}$ denote the transpose, the transpose-conjugate, and the inverse operations, respectively. $\|\mathbf{a}\|$ is the norm of a vector $\mathbf{a}$. $\odot$ denotes the Hadamard product. $\mathbb{E}\{\cdot\}$ represents statistical expectation. $\mathrm{Rank}(\cdot)$ and $\mathrm{Tr}\{\cdot\}$ denote the rank and the trace of matrix, respectively. $\mathbf{A}(i,j)$ denotes the element of the i-th row and the j-th column of matrix $\mathbf{A}$ and $\mathbf{a}(i)$ denotes the i-th element of vector $\mathbf{a}$.

II. System Model

We consider an IRS-assisted uplink OFDM system with N subcarriers, where both the access point (AP) and the user are equipped with single antenna as shown in Fig. 1. By connecting with a smart controller, an IRS composed of M elements can work collaboratively with the AP to intelligently enhance propagation. Denote $\mathcal{N} = \{1, \cdots, N\}$ and $\mathcal{M} = \{1, \cdots, M\}$ as the set of the indices of subcarriers and elements of the IRS, respectively. Moreover, in this paper, we assume all the links to be quasi-static frequency-selective fading channels.

Let $\mathbf{H}_{\mathrm{a}} \in \mathbb{C}^{M\times N}$, $\mathbf{H}_{\mathrm{u}} \in \mathbb{C}^{M\times N}$, and $\mathbf{h}_{\mathrm{d}} \in \mathbb{C}^{N}$ denote the channel frequency response (CFR) of AP-IRS link, IRS-user link, as well as AP-user link, respectively. $\mathbf{G} \triangleq \mathbf{H}_{\mathrm{u}} \odot \mathbf{H}_{\mathrm{a}} \in \mathbb{C}^{M\times N}$ denotes the CFR of user-IRS-AP cascade link (i.e., the dashed line in Fig. 1). Let $\mathbf{x} = [x_1, \cdots, x_N]^T \in \mathbb{C}^N$ denote the transmitted OFDM symbol in frequency domain at the user side, and $P_{\mathrm{t}} = \mathbb{E}\{\mathbf{x}^H\mathbf{x}\}$ denote the total transmit power. Then, the communication process can be described as follows: The transmitted OFDM symbol $\mathbf{x}$ is firstly transformed into time domain via an N-point inverse discrete fourier transform (IDFT), and then appended by a cyclic prefix (CP) of length L_{cp} to mitigate the inter-symbol-interference (ISI) in our considered wideband channels modeled by an L-tap finite-duration impulse response ($L_{\mathrm{cp}} \geq L$) [12]. At the receiver side, by removing the CP and performing an N-point DFT, the typical formulation of equivalent frequency-domain received signal at the n-th subcarrier y_n, $\forall n \in \mathcal{N}$, can be given as:

$$\begin{aligned} y_n &= (\mathbf{h}_{\mathrm{u},n}^H \mathrm{diag}(\boldsymbol{\phi}_n)\mathbf{h}_{\mathrm{a},n} + h_{\mathrm{d},n})x_n + v_n, \\ &= (\mathbf{g}_n^H \boldsymbol{\phi}_n + h_{\mathrm{d},n})x_n + v_n, \\ &\overset{(a)}{=} \widehat{\mathbf{g}}_n^H \boldsymbol{\psi}_n x_n + v_n, \end{aligned} \tag{1}$$

where $h_{\mathrm{d},n}$ denotes the n-th element of $\mathbf{h}_{\mathrm{d}}$. $\mathbf{h}_{\mathrm{u},n} \in \mathbb{C}^M$, $\mathbf{h}_{\mathrm{a},n} \in \mathbb{C}^M$ and $\mathbf{g}_n \triangleq \mathbf{h}_{\mathrm{u},n} \odot \mathbf{h}_{\mathrm{a},n} \in \mathbb{C}^M$ are the n-th column of $\mathbf{H}_{\mathrm{u}}$, $\mathbf{H}_{\mathrm{a}}$ and $\mathbf{G}$, respectively. $v_n \sim$

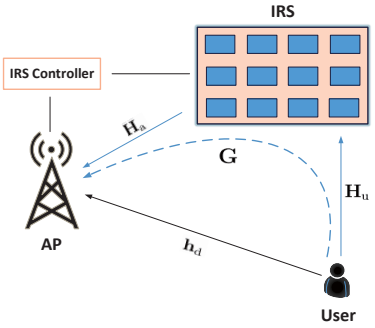

Fig. 1. An IRS-assisted uplink OFDM system.

$\mathcal{CN}(0, \sigma^2)$ is the additive Gaussian noise. Define $\boldsymbol{\phi}_n \triangleq [\beta_{n,1}e^{j\phi_{n,1}}, \cdots, \beta_{n,M}e^{j\phi_{n,M}}]^T \in \mathbb{C}^M$ as the IRS reflection coefficients at n-th subcarrier. Here, $\beta_{n,m}$ and $\phi_{n,m}$ denote the amplitude attenuation and phase shifts generated by m-th element corresponding to n-th subcarrier, respectively. And (a) follows by defining $\widehat{\mathbf{g}}_n^H \triangleq [h_{\mathrm{d},n}^H, \mathbf{g}_n^H] \in \mathbb{C}^{1\times(M+1)}$, $\boldsymbol{\psi}_n \triangleq \left[1, \boldsymbol{\phi}_n^H\right]^H \in \mathbb{C}^{M+1}$. In the prior works on the channel estimation for IRS-assisted OFDM systems, IRS is assumed to have an ideal reflection model: Reflection coefficients for different subcarriers are considered to be the same, i.e., $\beta_{1,m} = \cdots = \beta_{n,m} = 1$, $\phi_{1,m} = \cdots = \phi_{N,m}$, $\forall m \in \mathcal{M}$. However, according recent works [15], [16] reveal that it is not appropriate and also impractical to make this simple assumption. Specifically, the electrical characteristics of an IRS element is illustrated by a parallel resonant circuit and its reflection coefficients are essentially determined by the equivalent impedance. The value of impedance not only depends on the circuit parameters (e.g., the equivalent capacitance), but also relates to the frequency of incident signal. This means that the same IRS element with certain circuit parameters generates different responses (i.e. reflection coefficients) to signals with different frequencies. Thus, for wideband channels, the amplitude and the phase shift of an IRS element must vary with different subcarriers. In [15], the authors have successfully analyzed the mathematical formulation between the reflection coefficients of IRS and the frequency of the incident signal. Specifically, if we know the phase shift of an element at carrier frequency f_{c} of the total bandwidth B, then the corresponding reflection coefficients generated by the element at different subcarriers can be derived subsequently, which is given by [15]:

$$A(\phi_{\mathrm{c}}, f_n) = -\frac{\alpha_4\phi_{\mathrm{c}} + \alpha_5}{\left(\left(f_n/10^9 - \mathcal{D}_1\left(\phi_{\mathrm{c}}\right)\right)0.05\right)^2 + 4} + 1, , \forall n, \tag{2a}$$

$$W(\phi_{\mathrm{c}}, f_n) = -2\tan^{-1}[\mathcal{D}_2\left(\phi_{\mathrm{c}}\right)\left(f_n/10^9 - \mathcal{D}_1\left(\phi_{\mathrm{c}}\right)\right)], \forall n, \tag{2b}$$

$$\mathcal{D}_1(\phi_{\mathrm{c}}) = \alpha_1\tan(\phi_{\mathrm{c}}/3) + \alpha_2\sin(\phi_{\mathrm{c}}) + \alpha_6, \forall n, \tag{2c}$$

$$\mathcal{D}_2(\phi_{\mathrm{c}}) = \alpha_3\phi_{\mathrm{c}} + \alpha_7, \forall n, \tag{2d}$$

where ϕ_{c} denotes the phase shift corresponding to to carrier frequency f_{c}. f_n denotes the central frequency at the n-th subcarrier with $f_n \triangleq f_{\mathrm{c}} + \left(i - \frac{N+1}{2}\right)\frac{B}{N}, \forall n \in \mathcal{N}$. $A(\phi_{\mathrm{c}}, f_n)$ and $W(\phi_{\mathrm{c}}, f_n)$ are the function of ϕ_{c} and f_n, which denote the amplitude and phase shifts for subcarrier n, respectively.

$\alpha_1, \alpha_2, \alpha_3, \alpha_4, \alpha_5, \alpha_6, \alpha_7$ are the parameters which relates to specific circuit implementation. In practice, due to practical hardware implementation, the phase shift of each reflecting element can only take a finite number of discrete values [17]. Thus, in this paper we assume each reflecting element has finite-resolution phases controlled by bit b, whose set of values is given by:

$$\mathcal{F}_b = \{0, \Delta\omega, \cdots, (2^b - 1)\Delta\omega\}, \tag{3}$$

where $\Delta\omega = 2\pi/2^b$. Based on the above discussion, we further expand the signal model in the time domain, which will be utilized for the following channel estimation. Specifically, we define K time slots at each subcarrier and let $x_{n,k}$ denote the transmit symbol corresponding to n-th subcarrier at k-th time slot, $\forall n \in \mathcal{N}, k = 1, \cdots, K$. Then the received signal $\widehat{y}_{n,k}$ in our considered practical model during the k-th time slot at subcarrier n can be given as:

$$\widehat{y}_{n,k} = \widehat{\mathbf{g}}_n^H \boldsymbol{\psi}_{n,k} x_{n,k} + v_{n,k}, \forall n, \forall k, \tag{4}$$

where $\boldsymbol{\psi}_{n,k}$ denotes the time-expanded reflection vector corresponding to subcarrier n and time slot k, which is defined as: $\boldsymbol{\psi}_{n,k} \triangleq [1, \boldsymbol{\phi}_{n,k}^H]^H, \boldsymbol{\phi}_{n,k} \triangleq [\beta_{n,1,k} e^{j\phi_{n,1,k}}, \cdots, \beta_{n,M,k} e^{j\phi_{n,M,k}}]^T$. $\beta_{n,m,k}$ and $\phi_{n,m,k}$ denote the amplitude and phase shift of m-th element at the n-th subcarrier during k-th time slot, respectively, and they follow the relationship given in (2a)-(2d), i.e., $\beta_{n,m,k} = A(\phi_{\mathrm{c},m,k}, f_n)$, $\phi_{n,m,k} = W(\phi_{\mathrm{c},m,k}, f_n)$, $\forall n \in \mathcal{N}, \forall m \in \mathcal{M}, k = 1, \cdots, K$. $\phi_{\mathrm{c},m,k}$ denotes the phase shift of m-th element corresponding to f_c at k-th time slot. $v_{n,k}$ is the noise component at n-th subcarrier during k-th time slot.

In this paper, we aim to estimate the CFR of cascade link and direct link at all the subcarriers, i.e., $\widehat{\mathbf{g}}_n$, $\forall n \in \mathcal{N}$, at the AP. In the uplink training phase, the user consecutively sends K pilot symbols $x_{n,k}, k = 1, \cdots, K$, and each of which is associated with the pre-designed IRS reflection pattern (i.e., $\boldsymbol{\psi}_{n,k}$). Then the AP processes $\widehat{y}_{n,k}$ based on $x_{n,k}$ and $\boldsymbol{\psi}_{n,k}$, $\forall n \in \mathcal{N}$, $k = 1, \cdots K$, to perform the channel estimation. Since the accuracy of the estimated channel is tightly associated with the response of the IRS, the time-varying reflection pattern (i.e., $\boldsymbol{\psi}_{n,k}, \forall n \in \mathcal{N}, k = 1, \cdots, K$) of the IRS also needs to be properly designed to reduce the estimation errors. In the following two sections, we will describe the complete process of the channel estimation and provide the solutions of the reflection pattern design in details.

III. Proposed Channel Estimation Method and NMSE analysis

In this section, we propose a channel estimation method based on the practical IRS reflection model and give a concrete analysis about the NMSE of the estimated channels.

A. Proposed Channel Estimation Method

Before deriving the estimate of cascade link's CFR, we firstly need to perform the estimation of $\widehat{\mathbf{g}}_n \boldsymbol{\psi}_n$ during each training time slot. By right multiplying $x_{n,k}^{-1}$ by (4), the estimate of $\widehat{\mathbf{g}}_n \boldsymbol{\psi}_{n,k}$, denoted by $\widehat{z}_{n,k}$, can be formulated as:

$$\widehat{z}_{n,k} = \widehat{\mathbf{g}}_n^H \boldsymbol{\psi}_{n,k} + v_{n,k} x_{n,k}^{-1}, \forall n, \forall k. \tag{5}$$

Next, we seek to extract the estimate of $\widehat{\mathbf{g}}_n$ from $\widehat{z}_{n,k}$, $\forall n \in \mathcal{N}$, $k = 1, \cdots, K$. Based on the discussion in [6], we know that the number of transmitted pilot symbols needs to be no less than $M + 1$, so that the LS algorithm can be performed successfully. Therefore, the transmission protocol can be expressed as: *i)* The user side consecutively sends $K = M + 1$ OFDM symbols within one channel coherence time; *ii)* upon reflected by the IRS, the signal is received at the AP; *iii)* then, the AP derives $\widehat{z}_{n,k}$,$\forall n \in \mathcal{N}$, for each time slot based on (5); *iiii)* finally, the AP aggregates total K estimated $\widehat{\mathbf{g}}_n \boldsymbol{\psi}_{n,k}$ (i.e., $\widehat{z}_{n,k}, k = 1, \cdots, K$). If $\boldsymbol{\psi}_{n,k}, \forall n \in \mathcal{N}, k = 1, \cdots K$, are pre-defined, the estimation of $\widehat{\mathbf{g}}_n$ can be obtained at the AP directly based on the above protocol. Here, we define $\widehat{\mathbf{z}}_n \triangleq [\widehat{z}_{n,1}, \cdots, \widehat{z}_{n,K}]^H, \forall n \in \mathcal{N}$, as the aggregated $\widehat{z}_{n,k}$, which can be formulated as:

$$\widehat{\mathbf{z}}_n^H = \widehat{\mathbf{g}}_n^H \boldsymbol{\Psi}_n + \widehat{\mathbf{v}}_n^H, \forall n, \tag{6}$$

where

$$\boldsymbol{\Psi}_n = [\boldsymbol{\psi}_{n,1}, \cdots, \boldsymbol{\psi}_{n,K}], \forall n, \tag{7}$$

$$\begin{aligned} \widehat{\mathbf{v}}_n &= [v_{n,1} x_{n,1}^{-1}, \cdots, v_{n,k} x_{n,K}^{-1}]^H \\ &\overset{(b)}{=} (\mathrm{diag}(\widehat{\mathbf{x}}_n^{-1}))^H \widetilde{\mathbf{v}}_n, \forall n, \end{aligned} \tag{8}$$

and (b) holds by defining $\widetilde{\mathbf{v}}_n \triangleq [v_{n,1}, \cdots, v_{n,K}]^H$, $\widehat{\mathbf{x}}_n \triangleq [x_{n,1}, \cdots, x_{n,K}]^H$. If $\boldsymbol{\Psi}_n$ is full-rank, the LS estimation of $\widehat{\mathbf{g}}_n$ is performed by multiplying $\boldsymbol{\Psi}_n^{-1}$ on (6), which yields the estimated channel $\widetilde{\mathbf{g}}_n$ as:

$$\widetilde{\mathbf{g}}_n^H = \widehat{\mathbf{z}}_n^H \boldsymbol{\Psi}_n^{-1} = \widehat{\mathbf{g}}_n^H + \widehat{\mathbf{v}}_n^H \boldsymbol{\Psi}_n^{-1}, \forall n. \tag{9}$$

Now the protocol to estimate the CFR of cascade link and direct link for all subcarriers is established. In the following subsection, we will provide a theoretical derivation of the NMSE of estimated channels.

B. NMSE Analysis

In this subsection, we derive the NMSE of estimated channels, the formulation of which can be given as:

$$\mathrm{NMSE} = \frac{1}{N} \mathbb{E} \left\{ \frac{\sum_{n=1}^{N} \|\widetilde{\mathbf{g}}_n^H - \widehat{\mathbf{g}}_n^H\|^2}{\sum_{n=1}^{N} \|\widehat{\mathbf{g}}_n^H\|^2} \right\}. \tag{10}$$

It can be observed from equations (5)-(10) that the estimation errors $\widetilde{\mathbf{g}}_n^H - \widehat{\mathbf{g}}_n^H = \widehat{\mathbf{v}}_n \boldsymbol{\Psi}_n^{-1}$ are statistically independent of $\widehat{\mathbf{g}}_n^H$, thus (10) can be transformed as:

$$\begin{aligned} \mathrm{NMSE} &= \frac{1}{N} \frac{\sum_{n=1}^{N} \mathbb{E}\{\|\widetilde{\mathbf{g}}_n^H - \widehat{\mathbf{g}}_n^H\|^2\}}{\sum_{n=1}^{N} \mathbb{E}\{\|\widehat{\mathbf{g}}_n^H\|^2\}} \\ &= \frac{1}{N} \frac{\sum_{n=1}^{N} \mathrm{Tr}\left\{\mathbb{E}\{(\boldsymbol{\Psi}_n^{-1})^H \widehat{\mathbf{v}}_n \widehat{\mathbf{v}}_n^H \boldsymbol{\Psi}_n^{-1}\}\right\}}{\sum_{n=1}^{N} \mathbb{E}\{\|\widehat{\mathbf{g}}_n^H\|^2\}}, \end{aligned} \tag{11}$$

where

$$\begin{aligned}\mathrm{Tr}\left\{\mathbb{E}\{(\boldsymbol{\Psi}_n^{-1})^H\widehat{\mathbf{v}}_n\widehat{\mathbf{v}}_n^H\boldsymbol{\Psi}_n^{-1}\}\right\} &= \mathrm{Tr}\{(\boldsymbol{\Psi}_n^{-1})^H\mathbb{E}\{(\mathrm{diag}(\widehat{\mathbf{x}}_n^{-1}))^H \\ &\quad\times\widetilde{\mathbf{v}}_n(\widetilde{\mathbf{v}}_n)^H\mathrm{diag}(\widehat{\mathbf{x}}_n^{-1})\}\boldsymbol{\Psi}_n^{-1}\} \\ &= \frac{\sigma^2}{P_n}\mathrm{Tr}\left\{(\boldsymbol{\Psi}_n^{-1})^H\boldsymbol{\Psi}_n^{-1}\right\},\end{aligned} \tag{12}$$

and P_n denotes the average transmit power for the n-th subcarrier. Here, we assume the transmit power is equally allocated in each subcarrier, i.e., $P_n = \frac{P_\mathrm{t}}{N}$. Thus, (11) can be also written as:

$$\mathrm{NMSE} = \frac{\sigma^2}{P_\mathrm{t}}\frac{\sum_{n=1}^{N}\mathrm{Tr}\{(\boldsymbol{\Psi}_n^{-1})^H\boldsymbol{\Psi}_n^{-1}\}}{\sum_{n=1}^{N}\mathbb{E}\{\|\widehat{\mathbf{g}}_n^H\|^2\}}. \tag{13}$$

From (13), we can conclude that the value of NMSE is heavily determined by $\boldsymbol{\Psi}_n$. If the reflection pattern $\boldsymbol{\Psi}_n$ is not properly constructed, the NMSE become quite high. Therefore, how to design a proper IRS time-varying reflection pattern is a crucial issue for channel estimation, which will be discussed in the next section.

IV. Reflection Pattern Design

In this section we address the problem of the IRS time-varying reflection pattern design to minimize NMSE. Although some recent works [11]-[13] have investigated on proper pattern design schemes, they mainly focus on channel estimation strategies based on ideal IRSs. When it comes to practical IRS-insisted situations, these methods cannot suit well anymore. From (13), we know that the value of NMSE is related to $\boldsymbol{\Psi}_n$ corresponding to different subcarriers. However, $\boldsymbol{\Psi}_n, \forall n \in \mathcal{N}$, cannot be designed individually. Specifically, during each training time slot, the response of practical IRS (i.e., the selecting of an appropriate capacitance) are tuned according to one frequency, which yields different responses to signals with different frequencies. Here, we consider the reflection pattern design focusing on the carrier frequency of the total bandwidth (i.e., f_c). Therefore, our objective is formulated as properly designing the reflection pattern at f_c to minimize NMSE derived in the previous section. Let $\boldsymbol{\Phi}_\mathrm{c}$ denote the time-varying reflection pattern matrix corresponding to f_c, $\boldsymbol{\Phi}_\mathrm{c} \triangleq [\boldsymbol{\theta}_1, \cdots, \boldsymbol{\theta}_K]$, $\boldsymbol{\theta}_k \triangleq [1, \phi_{\mathrm{c},1,k}, \cdots, \phi_{\mathrm{c},M,k}]^T$, $k = 1, \cdots, K$. Then the reflection pattern design problem is given by:

$$\min_{\boldsymbol{\Phi}_\mathrm{c}} \sum_{n=1}^{N}\mathrm{Tr}\{(\boldsymbol{\Psi}_n^{-1})^H\boldsymbol{\Psi}_n^{-1}\} \tag{14a}$$

$$\text{s.t. } \mathrm{Rank}(\boldsymbol{\Psi}_n) = M+1, \forall n, \tag{14b}$$

$$\boldsymbol{\Psi}_n(1,:) = \mathbf{1}_{1\times(M+1)}, \forall n, \tag{14c}$$

$$\beta_{n,m,k} = A(\phi_{\mathrm{c},m,k}, f_n), \forall n, \forall m, \forall k, \tag{14d}$$

$$\phi_{n,m,k} = W(\phi_{\mathrm{c},m,k}, f_n), \forall n, \forall m, \forall k, \tag{14e}$$

$$\phi_{\mathrm{c},m,k} \in \mathcal{F}_b, \forall m, \forall k, \tag{14f}$$

where (14b) is a restriction to assure the existence of $\boldsymbol{\Psi}_n^{-1}$, and (14c) is derived based on the definition of $\boldsymbol{\psi}_n$. Obviously, this is a both non-convex and complicated problem, which cannot be solved directly. To effectively and efficiently cope with this difficulty, we firstly obtain the solution of $\boldsymbol{\Phi}_\mathrm{c}$ by leveraging AO [3] technique for the case of employing to low-resolution phase shifters to realize practical IRS (i.e., b = 1, 2). Then, we extend our analysis for high-resolution IRS cases (i.e., $b \geq 3$) and modify the practical reflection pattern design scheme to efficiently calculate $\boldsymbol{\Phi}_\mathrm{c}$.

Algorithm 1 AO-based Low-Resolution Reflection Pattern Design

Input: M, N, b.
Output: $\boldsymbol{\Phi}_\mathrm{c}$.

```
Initialize Φ_c^(0) according to [8].
for iter = 1 : S_max do
    for i = 2 to M + 1 do
        for j = 1 to M + 1 do
            Update Φ_c(i, j) by solving problem (15).
        end for
    end for
end for
Φ_c = Φ_c^(iter).
```

A. Low-Resolution IRS Cases

In this subsection, we begin with using AO algorithm to find the optimal $\boldsymbol{\Phi}_\mathrm{c}$ to construct the desired reflection pattern for low-resolution IRS cases. Given an initial value of $\boldsymbol{\Phi}_\mathrm{c}$, we aim to successively update each element for the reflection pattern matrix. Specifically for the design of $\boldsymbol{\Phi}_\mathrm{c}(i,j), i = 2, \cdots, M+1, j = 1, \cdots, M+1$, we attempt to conditionally minimize the NMSE with fixed other elements of $\boldsymbol{\Phi}_\mathrm{c}$, i.e.,

$$\boldsymbol{\Phi}_\mathrm{c}(i,j) = \arg\min_{\boldsymbol{\Phi}_\mathrm{c}(i,j)\in\mathcal{F}_b}\sum_{n=1}^{N}\mathrm{Tr}\{(\boldsymbol{\Psi}_n^{-1})^H\boldsymbol{\Psi}_n^{-1}\}, \forall i, \forall j. \tag{15}$$

Thanks to the employment of low-resolution phase shifters for practical IRS realization, we can perform a low-complexity one-dimensional exhaustive search over the set $\mathcal{F}_b$. The above process will be repeatedly executed until the number of iterations equals to S_{max}. Here, S_{max} is set properly to guarantee the convergence of the total procedure, and the value of it will be discussed in Section V. It is worth noting that the initial value of the reflection pattern will, to a large extent, influence the performance of this kind of AO algorithm. Thus, we also need to set an appropriate initial $\boldsymbol{\Phi}_\mathrm{c}^{(0)}$. In this paper, we utilize the DFT-hadamard matrix scheme for discrete phase shifts in [8] as an initial value of $\boldsymbol{\Phi}_\mathrm{c}$. The above process is summarized in Algorithm 1.

Although the above AO technique is much superior as compared to exhaust search, at least $2^b M(M+1)$ searching times are needed to obtain the solution of $\boldsymbol{\Phi}_\mathrm{c}$, which will cause too much computation complexity if b is larger (i.e., $b \geq 3$), Thus, in the following subsection, we attempt to add a further modification based on our proposed AO-based algorithm in order to better suit for high-resolution IRS cases.

B. High-Resolution IRS Cases

In this subsection, we propose to further modify Algorithm 1 based on numerous numerical experiments to effectively

Algorithm 2 Practical High-Resolution Reflection Pattern Design

Input: M, N, b.
Output: $\mathbf{\Phi}_{\mathrm{c}}$.

```
Initialize Φ_c = Φ_c^2.
for b_1 = 2 : b do
    Update F_{b_1} by (3).
    for i = 2 : (M + 1) do
        for j = 1 : (M + 1) do
            Find q with F_{b_1}[q] = Φ_c(i, j).
            Update S_q.
            Obtain Φ_c(i, j) by solving problem (16).
        end for
    end for
end for
```

reduce the complexity for the practical high-resolution reflection pattern design scheme. Specifically, we try to explore the characteristic of the reflection pattern matrix obtained by Algorithm 1 and find that there exists some regularities between b-bit reflection matrix $\mathbf{\Phi}_{\mathrm{c}}^{b}$ and the $(b+1)$-bit one $\mathbf{\Phi}_{\mathrm{c}}^{b+1}$: If we obtain a certain angle $\mathcal{F}_{b+1}[q]$, which denotes the q-th element of the set $\mathcal{F}_{b+1}$, as the (i,j)-th element of $\mathbf{\Phi}_{\mathrm{c}}^{b}$ based on Algorithm 1, i.e., $\mathbf{\Phi}_{\mathrm{c}}^{b}(i,j)=\mathcal{F}_{b+1}[q]$, the value of $\mathbf{\Phi}_{\mathrm{c}}^{b+1}(i,j)$ is always set within a range $\mathcal{S}_q \triangleq \{\mathcal{F}_{b+1}[q-1], \mathcal{F}_{b+1}[q], \mathcal{F}_{b+1}[q+1]\}$, which includes the angle $\mathcal{F}_{b+1}[q]$ and its neighbors. Motivated by this finding, we can efficiently search the optimal $\mathbf{\Phi}_{\mathrm{c}}^{b+1}$ based on $\mathbf{\Phi}_{\mathrm{c}}^{b}$ and the corresponding set $\mathcal{S}_q$, i.e.,

$$\mathbf{\Phi}_{\mathrm{c}}(i,j) = \arg \min_{\mathbf{\Phi}_{\mathrm{c}}(i,j)\in\mathcal{S}_q} \sum_{n=1}^{N} \mathrm{Tr}\{(\mathbf{\Psi}_n^{-1})^H \mathbf{\Psi}_n^{-1}\}, \forall i, \forall j. \quad (16)$$

By repeating this step over all elements, the reflection pattern matrix can be obtained. The process is fully described in Algorithm 2. In this way, we only need to search $2bM(M+1)$ times to construct $\mathbf{\Phi}_{\mathrm{c}}$ instead of 2^b, which can, to a large extent, reduce the complexity as compared to Algorithm 1.

V. Simulation Results

In this section, some simulation results are provided to validate the effectiveness of our proposed channel estimation methods and reflection pattern design schemes. We consider an IRS-aided single-user OFDM system, with a single antenna at AP and an IRS of 36 elements. Both the horizontal distance from AP to IRS link and AP to user is set as 50 meters, while the vertical distance between IRS and user is 2 meters. Moreover, we assume all the links follow Rayleigh fading and the reference channel power gain at a distance of 1 m is -30dB. The pass loss exponents of AP-IRS link, IRS-user link, and AP-user link are set as 2.2, 2.4, and 3.5, respectively. The noise power σ^2 is set as -80dBm. The transmit OFDM symbol at the n-th subcarrier during k-th time slot satisfies $x_{n,k} = \sqrt{P_{\mathrm{t}}/N} e^{jw_{n,k}}$, where $w_{n,k}$ is the random phase uniformly distributed within the range of [0,2π). The specific value of $\alpha_1, \alpha_2, \alpha_3, \alpha_4, \alpha_5, \alpha_6, \alpha_7$ are set according to [15]. Other parameters are set as follows: $f_{\mathrm{c}} = 2.4$GHz, $N = 64$, $B = 0.2$GHz, $L = 8$, and $L_{cp} = 16$.

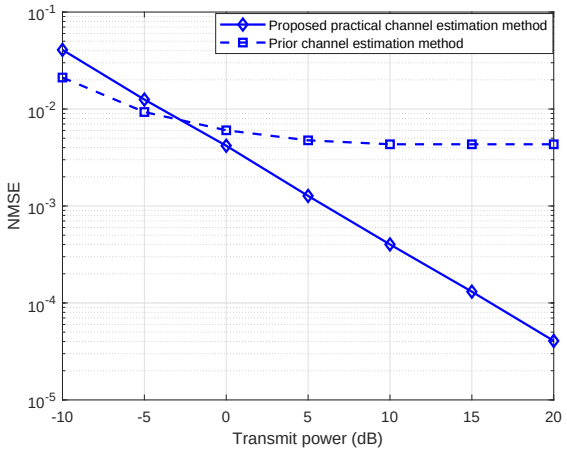

Fig. 2. NMSE versus transmit power under existing reflection pattern design schemes ($b = 5$).

We firstly examine the necessity of taking the practical response of IRS into consideration for channel estimation. In Fig. 2, we plot the NMSE versus transmit power under our proposed practical channel estimation methods by using the existing reflecting pattern design for discrete phase shifts (i.e., DFT-hadamard-matrix design proposed in [8]). In addition, we perform channel estimation by using the prior channel estimation method, i.e., the signals for different frequencies share the same reflection pattern. As the transmit power becomes larger, it is observed that the NMSE decreases drastically when executing our proposed practical channel estimation method. By contrast, the NMSE based on the prior channel estimation methods achieves a worse performance and the value of its NMSE doesn't decrease effectively with increasing transmit power. The gap between these two schemes gets much larger with the growth of transmit power.

Next, we evaluate the covergence of our proposed Algorithm 1 by plotting the value of (14a) versus the number of iterations for the case of employing 1-bit resolution phase shifters. In the top sub-figure of Fig. 3, it can be observed that Algorithm 1 can converge within limited iterations, (i.e., within 2 iterations). Thus, in this paper, we set $S_{max} = 2$ directly to improve the efficiency of calculating. Then in the bottom sub-figure of Fig. 3, we examine the effectiveness of our proposed Algorithm 2 and plot the value of objective (14a) as a function of resolution b for each IRS element. From this sub-figure we can see that $b = 5$ is a sufficient resolution since the decrease of NMSE is marginal when $b \geq 5$.

Finally, we show the superior performance of our proposed reflection pattern design schemes. In Fig. 4, we plot the NMSE versus transmit power for the scenarios with different resolution bits, under our proposed AO-based low-resolution reflection pattern design (i.e., Algorithm 1) and practical high-resolution reflection pattern design (i.e., Algorithm 2). For comparison, we also add DFT-hadamard-matrix based design proposed in [8] as the benchmark. It can be observed in Fig. 4 that the proposed schemes always achieve much better performance for all transmit power ranges. Compared with the DFT-hadamard-matrix based method, our proposed reflection

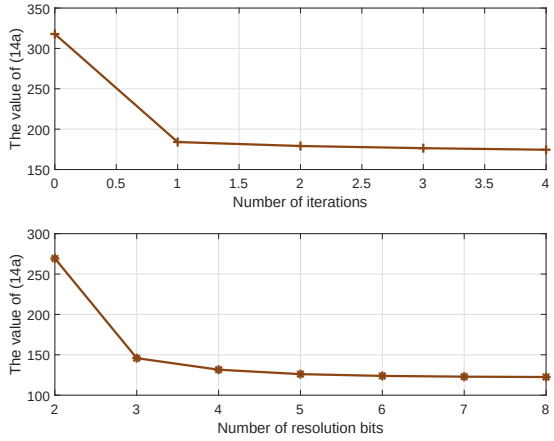

Fig. 3. Top: The value of (14a) versus the number of iterations based on Algorithm 1, $b = 1$. Bottom: The value of (14a) versus the resolution b based on Algorithm 2.

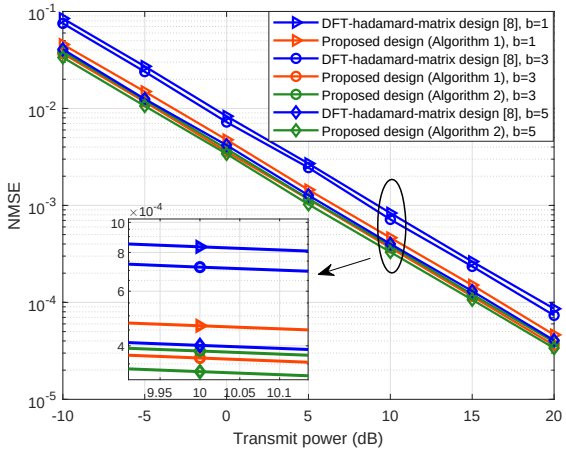

Fig. 4. NMSE versus transmit power for low-resolution IRS cases and high-resolution IRS cases.

pattern design schemes can dramatically low the NMSE, e.g., decrease by 46 % and 37 % for low-resolution IRS cases ($b = 1$) and high-resolution IRS cases ($b \geq 3$), respectively. Moreover, to further demonstrate the feasibility of the proposed practical high-resolution reflection pattern design, we also compare the NMSE by using proposed Algorithm 1 to obtain the solution of reflecting pattern when $b = 3$. It can be observed that our proposed practical reflection pattern design (i.e., Algorithm 2) can achieve almost the same performance as Algorithm 1, but can largely reduce the computational complexity greatly due to the narrower searching range, especially for the systems with high resolution bits, which illustrate the effectiveness and efficiency of our proposed design.

VI. Conclusions

In this paper, we firstly proposed a novel channel estimation method for IRS-assisted wideband OFDM systems by considering IRS with a practical reflection model. Then, we designed a proper IRS time-varying reflecting pattern based on AO algorithm to minimize the NMSE for low-resolution IRS cases. To further improve the computational efficiency in designing reflecting pattern for the case of using high resolution phase shifters, another practical high-resolution reflection pattern design scheme was proposed. Simulation results demonstrated the effectiveness of our proposed methods.

References

[1] M. Di Renzo, A. Zappone, M. Debbah, M.-S. Alouini, C. Yuen, J. de Rosny, and S. Tretyakov, "Smart radio environments empowered by reconfigurable intelligent surfaces: How it works, state of research, and road ahead," *IEEE J. Sel. Areas Commun.*, vol. 38, no. 11, pp. 2450-2525, Nov. 2020.

[2] Q. Wu, S. Zhang, B. Zheng, C. You, and R. Zhang, "Intelligent reflecting surface aided wireless communications: A tutorial," July 2020. [Online]. Available: https://arxiv.org/abs/2007.02759.

[3] Q. Wu and R. Zhang, "Intelligent reflecting surface enhanced wireless network via joint active and passive beamforming," *IEEE Trans. Wireless Commun.*, vol. 18, no. 11, pp. 5394-5409, Nov. 2019.

[4] B. Lyu, D. Hoang, S. Gong, D. Niyato, and D. Kim, "IRS-based wireless jamming attacks: When jammers can attack without power," *IEEE Commun. Lett.*, vol. 9, no. 10, pp. 1663-1667, Oct. 2020.

[5] Q. Nadeem, A. Kammoun, A. Chaaban, M. Debbah, and M. Alouini, "Intelligent reflecting surface assisted wireless communication: Modeling and channel estimation," June 2019. [Online]. Available: https://arxiv.org/abs/1906.02360.

[6] Z. Wang, L. Liu, and S. Cui, "Channel estimation for intelligent reflecting surface assisted multiuser communications: Framework, algorithms, and analysis," *IEEE Trans. Wireless Commun.*, vol. 19, no. 10, pp. 6607-6620, Oct. 2020.

[7] Q. Nadeem, H. Alwazani, A. Kammoun, A. Chaaban, M. Debbah, and M. Alouini, "Intelligent reflecting surface-assisted multi-user MISO communication: Channel estimation and beamforming design," *IEEE Open J. Commun. Soc.*, vol. 1, pp. 661-680, 2020.

[8] C. You, B. Zheng, and R. Zhang, "Intelligent reflecting surface with discrete phase shifts: Channel estimation and passive beamforming," in *Proc. IEEE Int. Conf. Commun. (ICC)*, Virtual Conference, June 2020, pp. 1-6.

[9] X. Guan, Q. Wu, and R. Zhang, "Anchor-assisted intelligent reflecting surface channel estimation for multiuser communications," Aug. 2020. [Online]. Available: https://arxiv.org/abs/2008.00622.

[10] J. Kang, "Intelligent reflecting surface: Joint optimal training sequence and refection pattern," *IEEE Commun. Lett.*, vol. 24, no. 8, pp. 1784-1788, Aug. 2020.

[11] Y. Yang, B. Zheng, S. Zhang, and R. Zhang, "Intelligent reflecting surface meets OFDM: Protocol design and rate maximization," *IEEE Trans. Commun.*, vol. 68, no. 7, pp. 4522-4535, July 2020.

[12] B. Zheng and R. Zhang, "Intelligent reflecting surface-enhanced OFDM: Channel estimation and reflection optimization," *IEEE Commun. Lett.*, vol. 9, no. 4, pp. 518-522, April 2020.

[13] B. Zheng, C. You, and R. Zhang, "Fast channel estimation for IRS-assisted OFDM," Aug. 2020. [Online]. Available: https://arxiv.org/abs/2008.04476.

[14] A. Elbir and S. Coleri, "Federated learning for channel estimation in conventional and IRS-assisted massive MIMO," Aug. 2020. [Online]. Available: https://arxiv.org/abs/2008.10846.

[15] W. Cai, H. Li, M. Li, and Q. Liu, "Practical modeling and beamforming for intelligent reflecting surface aided wideband systems," *IEEE Commun. Lett.*, vol. 24, no. 7, pp. 1568-1571, July 2020.

[16] H. Li, W. Cai, Y. Liu, M. Li, and Q. Liu, "Intelligent reflecting surface enhanced wideband MIMO-OFDM communications: From practical model to reflection optimization," July 2020. [Online]. Available: https://arxiv.org/abs/2007.14243.

[17] Q. Wu and R. Zhang, "Beamforming optimization for wireless network aided by intelligent reflecting surface with discrete phase shifts," *IEEE Trans. Commun.*, vol. 68, no. 3, pp. 1838-1851, March 2020.